Evidence of large spin-orbit coupling effects in quasi-free-standing graphene on Pb/Ir(1 1 1)

2D Materials

OPEN ACCESS

RECEIVED
31 December 2017

REVISED
8 May 2018

ACCEPTED FOR PUBLICATION
17 May 2018

PUBLISHED
4 June 2018

PAPER

Evidence of large spin-orbit coupling effects in quasi-free-standing graphene on Pb/Ir(1 1 1)

M M Otrokov[1,2], I I Klimovskikh[3], F Calleja[4], A M Shikin[3], O Vilkov[3], A G Rybkin[3], D Estyunin[3], S Muff[5,6], J H Dil[5,6], A L Vázquez de Parga[4,7], R Miranda[4,7], H Ochoa[8], F Guinea[4,9], J I Cerdá[10], E V Chulkov[1,3,11,12] and A Arnau[1,11,12]

[1] Centro de Física de Materiales (CFM-MPC), Centro Mixto CSIC-UPV/EHU, 20018 Donostia-San Sebastián, Basque Country, Spain
[2] Tomsk State University, 634050 Tomsk, Russia
[3] Saint Petersburg State University, 198504 Saint Petersburg, Russia
[4] Instituto Madrileño de Estudios Avanzados en Nanociencia, Cantoblanco 28049, Madrid, Spain
[5] Institute of Physics, Ecole Polytechnique Fédérale de Lausanne, CH-1015 Lausanne, Switzerland
[6] Swiss Light Source, Paul Scherrer Institut, CH-5232 Villigen, Switzerland
[7] Departamento de Física de la Materia Condensada and IFIMAC, Universidad Autónoma de Madrid, Cantoblanco 28049, Madrid, Spain
[8] Department of Physics and Astronomy, University of California, Los Angeles, CA 90095, United States of America
[9] Department of Physics and Astronomy, University of Manchester, Oxford Road, Manchester M13 9PL, United Kingdom
[10] Instituto de Ciencia de Materiales de Madrid, Consejo Superior de Investigaciones Científicas, Cantoblanco 28049, Madrid, Spain
[11] Donostia International Physics Center (DIPC), 20018 Donostia-San Sebastián, Basque Country, Spain
[12] Departamento de Física de Materiales UPV/EHU, 20080 Donostia-San Sebastián, Basque Country, Spain

E-mail: mikhail.otrokov@gmail.com

Keywords: graphene, spin–orbit coupling, electronic structure, intercalation, scanning tunneling microscopy, angle-resolved photoemission spectroscopy, density functional theory

Supplementary material for this article is available online

Abstract

A combined scanning tunneling microscopy, angle- and spin-resolved photoemission spectroscopy and density functional theory study of graphene on Ir(1 1 1) intercalated with a well-ordered, full Pb monolayer is presented. Lead intercalation between graphene and Ir(1 1 1) reduces the coupling to the metallic substrate in such a way that its corrugation becomes negligible and distortions of the linear dispersion largely disappear, while graphene's sublattice symmetry is maintained and it turns out to be *n*-doped. Remarkably, the spin–orbit splittings induced by the proximity of the Ir(1 1 1) surface are preserved after Pb intercalation in a wide energy range. We further show that the Pb/Ir(1 1 1) surface induces a complex spin texture with both in-plane and out-of-plane components. Our calculations reveal the origin of the out-of-plane spin components in graphene to trace back to the out-of-plane spin-polarized surface and resonance states of Ir(1 1 1), while the Pb interlayer on its own does not induce any vertical spin polarization in the carbon sheet. However, the Brillouin zone folding imposed by the rectangular symmetry of the intercalated Pb layer plays an instrumental role in the spin–orbit coupling (SOC) transfer to graphene, as well as in the linearization of its bands. Finally, since no sizeable gap is observed at the Dirac point, we suggest that an intrinsic (Kane and Mele type) SOC does not exceed the extrinsic (Rashba) SOC for graphene on Pb/Ir(1 1 1).

1. Introduction

The spin–orbit coupling (SOC) is responsible for a surprising variety of intriguing phenomena in condensed matter physics [1, 2]. The effects due to SOC are especially prominent in reduced dimensions and new phases of matter, such as quantum spin and anomalous Hall states [3–8], Majorana fermions [9–11], skyrmions [12, 13], etc have emerged from the interplay between SOC and low dimensionality. This places 2D materials, thin films and heterostructures in a focus of intense research [14–18]. In particular, significant attention is being paid to the enhancement of SOC in graphene [19–32], which would be an important extension of its properties enabling a number of interesting applications. For example, if in addition to the unavoidable Rashba term, that appears in supported graphene [33–35], the substrate is magnetically ordered and induces an exchange coupling by proximity [36], then the system might

exhibit a quantum anomalous Hall effect [37]. On the contrary, if time-reversal symmetry is preserved but the intrinsic (Kane and Mele) SOC dominates, the system is ideally in a quantum spin Hall phase [3]. In graphene, a large value of the SOC and the corresponding spin–orbit splitting near the Dirac point (DP) could be incorporated either by proximity effects produced by placing graphene on appropriate substrates [19–22] or by intercalation [23–28] (adsorption [29–31]) of heavy atoms in the right geometry.

Experimentally, it is almost impossible to deposit adatoms on the surface of flat graphene in an ordered fashion. Additionally, the coupling strength between graphene and its support in epitaxial or intercalated systems has to be adjusted carefully: it cannot be too strong as graphene's exciting properties deriving from its linear dispersive bands would be lost. For example, the use of ferromagnetic substrates, like Fe, Co and Ni, permits to induce large exchange splittings in graphene bands, but their hybridization with the metal states is so strong that the Dirac cone is destroyed (at least in one of the spin channels) [38–41], unless a surface alloy is formed at the interface to tune the coupling strength [42]. Indeed, the intercalation of selected species between graphene and its metallic support is more amenable for structural control at the interface and it has been intensively explored [23–28]. In particular, when heavy atoms like Au or Pb are intercalated, graphene bands acquire spin–orbit splittings at different energies and regions of the surface Brillouin zone (BZ) but an ordered structure in the intercalated layer is not always achieved.

In general, the complex spin texture that appears in the electronic band structure is difficult to rationalize in terms of intrinsic (Kane and Mele type [3]) and extrinsic (Rashba [33]) SOC contributions, that are responsible for out-of-plane an in-plane spin polarizations, respectively, at least for planar systems. In graphene, an intrinsic term is required to give rise to the 2D topological insulator phase (quantum spin Hall state) and topologically protected spin-polarized edge states. For example, in the case of gr/Au/Ni(1 1 1) [23] the spin splitting induced in graphene near the DP has been understood as due to the Rashba effect only, while in gr/Pb/Pt(1 1 1) [26, 28] both an intrinsic SOC of the Kane and Mele type and a Rashba term have been suggested. Noteworthy, a coexistence of the exchange and spin–orbit splittings in the Dirac cone in graphene/Au/Co(0001) has been observed very recently [43]. Unfortunately, spin-resolved photoemission spectroscopy data do not always resolve both in-plane and out-of-plane spin components. Incidentally, a very recent alternative method to probe spin texture in topological surface states has been proposed by He *et al* [44], but it remains to be explored for other systems as well.

In this work, we consider the case of Pb intercalation between graphene and Ir(1 1 1) as in this system the Pb atoms form an ordered $c(4 \times 2)$ monolayer that decouples the carbon sheet from the substrate, resulting in an almost free-standing and perfectly flat graphene overlayer with preserved A–B sublattice symmetry, as observed by low temperature scanning tunneling microscopy (STM). Unlike [24], where spatially varying spin–orbit effects in gr/Ir(1 1 1) with small, ∼10 nm-wide, monolayer-thick Pb islands intercalated in between had been studied, here we concentrate on the large-scale domains of Pb-intercalated gr/Ir(1 1 1) and scrutinize its spin-resolved electronic structure. Our spin- and angle-resolved photoemission spectroscopy (ARPES) data, as well as first-principles density functional theory (DFT) calculations, show that in this system graphene coupling to the Pb/Ir(1 1 1) substrate has a sufficiently high value to induce large spin–orbit splittings as well as sizable both in-plane and out-of-plane spin components in the graphene π-bands near the $\overline{\mathrm{K}}$ point, while essentially maintaining the linear dispersion of the bands. In spite of the substantial out-of-plane spin polarization observed for the Pb-intercalated graphene bands, the absence of a gap at the DP indicates that the intrinsic (Kane and Mele type) SOC does not exceed the extrinsic (Rashba) SOC for graphene on Pb/Ir(1 1 1). Our first-principles DFT calculations permit to interpret and rationalize both the STM and ARPES observations.

2. Results and discussion

Pb-intercalated graphene on Ir(1 1 1) is known to show a moiré pattern with the same lateral periodicity as the well-known (9.3×9.3) superstructure of gr/Ir(1 1 1) [19, 25, 45], but with a much smaller corrugation [24] than the one observed (30 pm) on the moiré superstructure corresponding to gr/Ir(1 1 1). Below graphene, the Pb layer on Ir(1 1 1) forms three spatially separated rotational domains of a rectangular $c(4 \times 2)$ structure, commensurate with Ir(1 1 1) [24].

Figure 1(a) shows a representative, atomically resolved STM image acquired on a large monodomain in the gr/Pb/Ir(1 1 1) area. In the image, the hexagonal atomic lattice of graphene, the rectangular $c(4 \times 2)$ lattice of intercalated Pb [24] and the gr/Ir(1 1 1) moiré superstructure can be seen. This $c(4 \times 2)$ superstructure of Pb atoms on Ir(1 1 1) is identical to the one observed for direct deposition of Pb on Ir(1 1 1). Notice that the underlying Pb lattice is incommensurate with the graphene lattice above [24].

Figure 1(b) shows the 2D fast Fourier transform (FFT) of a large, atomically resolved STM image (shown in the supplementary note I (stacks.iop.org/TDM/5/035029/mmedia)), where, in addition to the moiré superspots of the underlying $c(4 \times 2)$ Pb monodomain, six half-moon circles at the $\sqrt{3}$ positions of the surface BZ of graphene are seen. The latter correspond to elastic intervalley scattering between two adjacent, non-equivalent Dirac cones in almost ideally isolated graphene produced by atomic-size defects [46, 47]. Their presence demonstrates that the Pb-

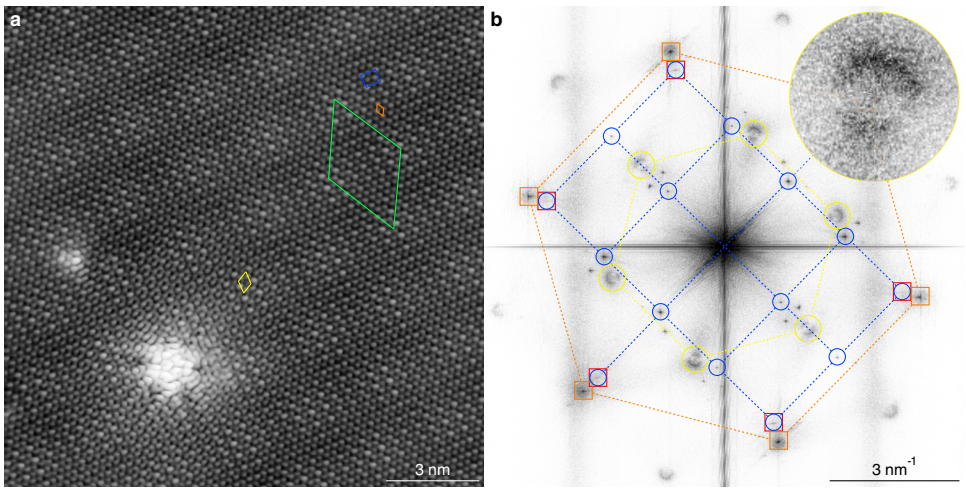

Figure 1. (a) Atomically resolved topographic STM image of Pb-intercalated gr/Ir(1 1 1) recorded at 4.6 K. The area selected contains an intervalley scattering center. The unit cells of graphene (orange), Pb (blue) and the one of the (9.3 × 9.3) moiré pattern (green) are highlighted in the upper right part of the image. The intervalley pattern close to the defect is highlighted in yellow. The image has been taken with a sample bias of -3 mV and 1 nA tunneling current; (b) FFT of a 175 × 175 nm^2 STM image recorded at a bias of -3 mV and 300 pA of tunneling current with a similar resolution as the one shown in panel (a). The spots corresponding to the unit cells of graphene (orange), Ir (red) and Pb (blue) are shown. The intervalley scattering rings are encircled in yellow and one of them is magnified in the inset.

intercalated graphene overlayer is further decoupled from the metallic substrate underneath, since they are not observed for pristine gr/Ir(1 1 1). The anisotropy in the intensity of the intervalley rings responsible for their half-moon appearance indicates that the symmetry between the A and B sublattices of graphene is preserved after the Pb intercalation [46, 47].

Overall, our STM and low energy electron diffraction (LEED, figure 2(a)) data indicate a well-ordered surface of gr/Pb/Ir(1 1 1) at large scale, a compulsory requisite to perform well-defined ARPES measurements. The detailed adsorption geometry (i.e. adsorption site and bond distance) of Pb/Ir(1 1 1) cannot be determined neither from the symmetry of the LEED pattern nor from the FFT of the large scale atomically resolved STM image. However, our structural total-energy DFT calculations reveal that Pb atoms adsorbed on Ir(1 1 1) show a slight preference for the fcc threefold hollow sites over the hcp sites, while the bridge and especially top positions are by far more unfavourable. Further calculations allow us to conclude that graphene appears to be physisorbed on the Ir-supported Pb layer at an average distance of about 3.3–3.4 Å from the Pb atoms.

A set of ARPES images of gr/Pb/Ir(1 1 1) acquired slightly off the $\overline{\mathrm{K}}$ point (outer images) and exactly at $\overline{\mathrm{K}}$ (middle image) is presented in figure 2(b). The middle image of figure 2(b) is shown frontally in figure 2(c), where the direction of measurement is indicated in the panel at the bottom part. A linearly-dispersing π state indicates a quasi-free-standing character of the Pb-intercalated graphene on Ir(1 1 1), in agreement with our DFT calculations (see below). The estimated position of the DP corresponds to the crossing of the two dashed lines at ∼250 meV below the Fermi level, as shown in the figure. This value is in qualitative agreement with the scanning tunneling spectroscopy data in [24] that show a DP at ∼110 meV below the Fermi level for small lead islands intercalated below graphene on Ir(1 1 1). The peak in the EDC taken exactly at the $\overline{\mathrm{K}}$ point (figure 2(d)) can be fitted with a single broad peak, consistent with the absence of a sizable gap at the DP. Due to the limited energy resolution of the ARPES data, one cannot resolve the fine structure around the maximum at the DP binding energy. However, our EDC analysis (supplementary note II) allows concluding that the width of the graphene Dirac cone state is increased at the $\overline{\mathrm{K}}$ point by ∼140 meV, which is consistent with a SOC splitting dominated by a Rashba term assuming the absence of the DP gap, as we discuss below.

Spin-resolved ARPES data are shown in figures 3(a) and (b) for the π and π^* states, respectively. The measurements have been performed at $k_x = -0.13 \pm 0.03$ Å^{-1} and $k_x = +0.03 \pm 0.03$ Å^{-1} as indicated by blue transparent stripes at the inset. Spin-up and spin-down spectra are obtained using the total spin polarization, shown at the panel below (black symbols). Inspecting the spectra, one can see splittings of the order of 100 meV for the π (figure 3(a)) and 70 meV for the π^* (figure 3(b)) states. Note, that these values are affected by energy and angular resolution of the spin resolved ARPES measurements. Also, the determination of the splitting value is hampered for the π^* state due to the vicinity of the Fermi level. The in-plane and out-of-plane spin polarization components have similar values and behavior for both π and π^* states, as seen from the lower panels.

The measured spin splitting in gr/Pb/Ir(1 1 1) appears to be larger than in gr/Ir(1 1 1), for which values up to 50–60 meV have been reported [19]. However, the splitting of the Dirac cone observed for

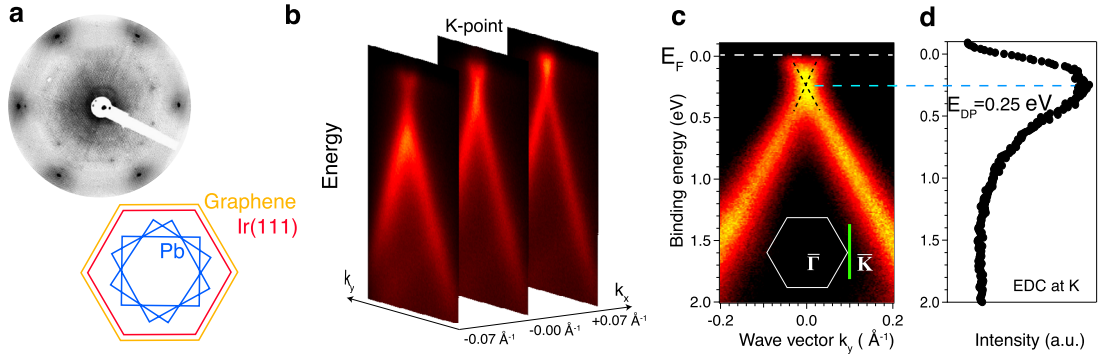

Figure 2. (a) LEED pattern of gr/Pb/Ir(1 1 1) obtained with an electron beam energy of 150 eV and the 2D reciprocal lattices of graphene, Pb $c(4 \times 2)$ and Ir(1 1 1) shown in orange, blue, and red, respectively. (b) Selected ARPES band dispersions acquired with a photon energy of 21.2 eV for gr/Pb/Ir(1 1 1) in two orthogonal directions in the k-space shown in (b) and (c). (c) Band dispersion through the $\overline{\mathrm{K}}$ point perpendicular to the $\overline{\Gamma\mathrm{K}}$ direction, as indicated in the inset. $k_y = 0$ corresponds to the $\overline{\mathrm{K}}$-point of the graphene BZ. (d) Energy distribution curve (EDC) for gr/Pb/Ir(1 1 1) at the $\overline{\mathrm{K}}$ point.

these two systems in the spin-resolved measurements is not seen in the spin-integrated spectra due to the large linewidth of the graphene π-states. Moreover, a comparative analysis of the EDCs, performed for the spin-integrated data acquired on both gr/Ir(1 1 1) and gr/Pb/Ir(1 1 1), shows that the linewidth of the π-state increases roughly twice after the Pb intercalation (from 280 to 520 meV, see supplementary note III). This enhancement of the peak width is related not only to the spin splitting, but also to both structural effects of Pb intercalation (e.g. Pb rotational domains, imperfections of the intercalated layer) and a modified hybridization of graphene bands with Pb/Ir(1 1 1), as the $c(4 \times 2)$ periodicity introduces a folding of Ir states that closes its projected band gap around $\overline{\mathrm{K}}$ (see the discussion of the band structure calculations below). Similar linewidth enhancement has been observed in [48] after a Bi layer intercalation underneath graphene on Ir(1 1 1) and has been ascribed to the surface lattice disorder introduced by intercalation and to the hybridization with the underlying Bi atoms.

Figure 4(a) shows the spin-integrated band structure calculated for a full monolayer of Pb-intercalated gr/Ir(1 1 1) in the form of a wave vector and energy resolved PDOS(k, E) after unfolding [49] from the (10×10) supercell to the (1×1) graphene surface unit cell (see supplementary note IV). The weak hybridization between graphene and Pb/Ir(1 1 1) bands manifests itself in an almost perfectly linear dispersion of the bands and the absence of a gap at the DP, while a significant n-doping effect placing the DP at about 250 meV below the Fermi level is apparent in very good agreement with ARPES data. A nontrivial spin texture appears as a result of the interaction between graphene and the underlying Pb/Ir(1 1 1) surface for both in-plane and out-of-plane spin components, as shown in figures 4(b) and (c). This non-planar spin texture suggests that both Rashba and Kane–Mele SOCs are induced in graphene. However, since no bandgap has been found at the DP, we suggest that the Kane and Mele contribution does not exceed the Rashba contribution [3]. Note that this particular Pb domain, for which the data shown in figure 4 have been obtained, does not induce the s_x spin component along k_x, while the other two Pb domains do. However, as we show in the supplementary note V, s_x components for those two domains turn out to be equal in magnitude but opposite in sign, while both s_y and s_z are equal in magnitude and have the same sign. Besides, the s_y and s_z components for the domain that does not induce s_x in graphene bands differ from those of the domains inducing it. From our LEED patterns as well as from the FFT STM images, acquired on the large scale, we can deduce that the three Pb domains appear in equal proportion at the Ir(1 1 1) surface as the intensity of the corresponding spots is very similar. The lateral size of the domains is typically smaller than 100 nm. Since in the spin-resolved ARPES the signal is collected from a much larger area (the spot size of about 100 microns), it is reasonable to expect that the s_x component vanishes (while s_y and s_z do not) when the measurement is performed along the k_x direction as it is done in our experiment. Unfortunately, fine details in the s_y and s_z spin texture corresponding to different Pb domains at present cannot be resolved even with state-of-the-art spin-ARPES measurements.

The magnitudes of the calculated spin splittings can be extracted from the spin density maps by examining energy distribution curves. The splittings were found to be k- and energy-dependent and to reach large values for graphene, although being significantly smaller than the measured ones, shown in figures 3(a) and (b). As it is shown in Supplementary Note VI, the maximal splitting reaches $\sim$30 meV for the π state along the $\overline{\Gamma\mathrm{K}}$ direction at $k_x = -0.14$ Å^{-1} counting from the $\overline{\mathrm{K}}$ point. Splittings of about 10 meV have been found for the π^* state.

At this point, before proceeding any further with the analysis of this complex spin texture, it is worth to compare with the results of a similar calculation, i. e. using the same (10×10) supercell, for gr/Ir(1 1 1). As can be seen by comparing figures 4 and 5, the main

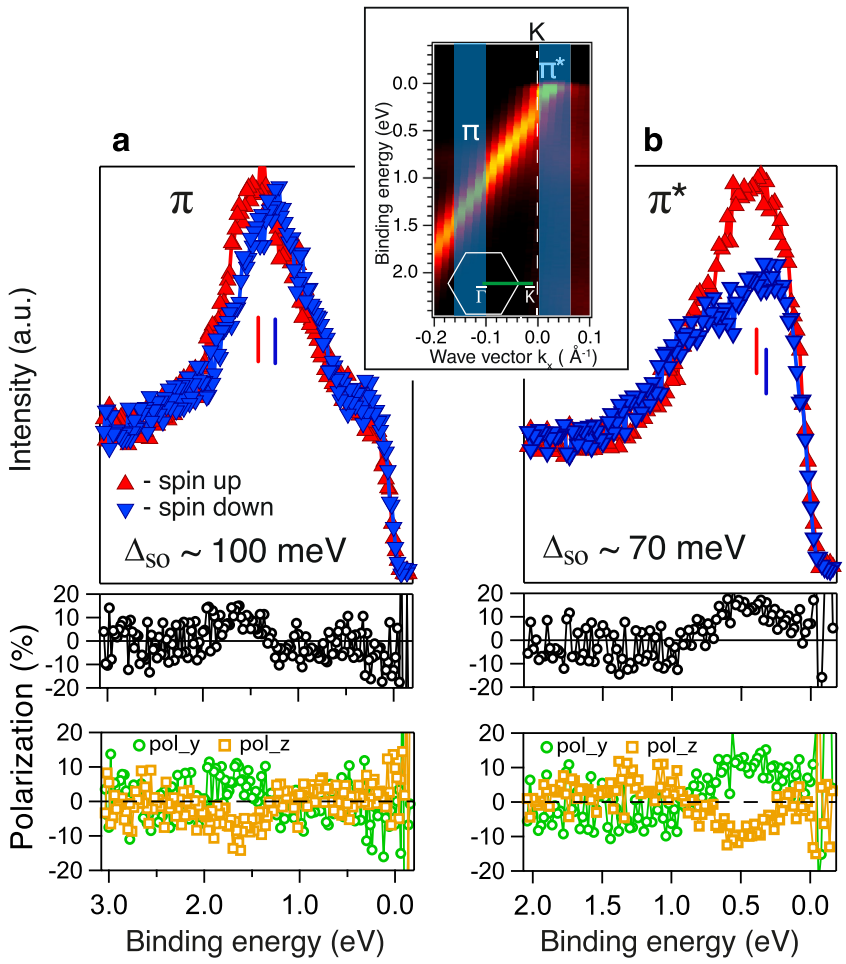

Figure 3. ((a), (b)) Spin-resolved ARPES spectra of gr/Pb/Ir(1 1 1) acquired with a photon energy of 72 eV along the $\overline{\Gamma KM}$ direction taken at two different emission angles. The spectra are obtained using the total spin polarization, calculated as a $sign(P_y) \times \sqrt{P_y^2 + P_z^2}$ (see methods section for more details) and displayed at the middle panels by black circles. Note, that we assume the $P_x = 0$ due to the reasons explained further in the text. The panels at the bottom show the spin polarization components along the y (green) and z (yellow) spin quantization axes. The inset shows the spin-integrated ARPES spectrum where the transparent blue stripes show the span of emission angles used to collect the spin-resolved data for the π and π^* states. $k_x = 0$ corresponds to the $\overline{K}$-point of the graphene BZ.

differences between the two systems are: (i) graphene is n- or p-doped on Pb/Ir(1 1 1) or Ir(1 1 1), being the DP at about −250 meV or +150 meV, respectively, in agreement with available ARPES data [25, 50, 51], and (ii) overall, graphene π bands are better defined in gr/Pb/Ir(1 1 1) as compared to gr/Ir(1 1 1), in the sense that their linear dispersion is better maintained. A stronger hybridization between graphene and Ir(1 1 1) is evident, as compared to Pb/Ir(1 1 1), simply by looking at the multiple hybridization gaps that appear in the eV energy range below the DP. However, in the two systems both in-plane and out-of-plane spin polarization of graphene π bands near DP appears, although the spin polarization of the upper cone in gr/Ir(1 1 1) is strongly suppressed due to hybridization with the (1 1 1) projected Ir bulk states that introduce a significant broadening [see supplementary note VII showing the location of the projected band gap near the $\overline{K}$ point for Ir(1 1 1)].

In order to understand this complex hybridization and the corresponding spin texture, we have performed auxiliary calculations for gr/Pb only and gr/Pb/Ir using a $c(4 \times 2)$ surface unit cell, in which the graphene lattice constant is stretched by ∼10% to force commensurability (hereinafter we refer to this stretched graphene as gr*). In these cases, we have considered three different Pb-C registries that correspond to Pb atoms in hollow, bridge and top positions with respect to the C atoms in the graphene lattice (supplementary note IV). Both hollow and bridge Pb-C registries preserve graphene's A–B sublattice symmetry while the top Pb-C registry does not. The bandstructure of the unsupported gr/Pb bilayer in the (10×10) cell, maintaining the A–B sublattice symmetry, has also been calculated.

For the gr*/Pb unsupported bilayer, our DFT calculations performed using the $c(4 \times 2)$ surface unit cell for three different Pb-C registries (top, hollow and bridge) confirm that only for the Pb-C top registry the out-of-plane spin polarization appears, as it should be, due to the breakdown of A–B sublattice symmetry [52] (see figure 6). The reason for that spin texture of

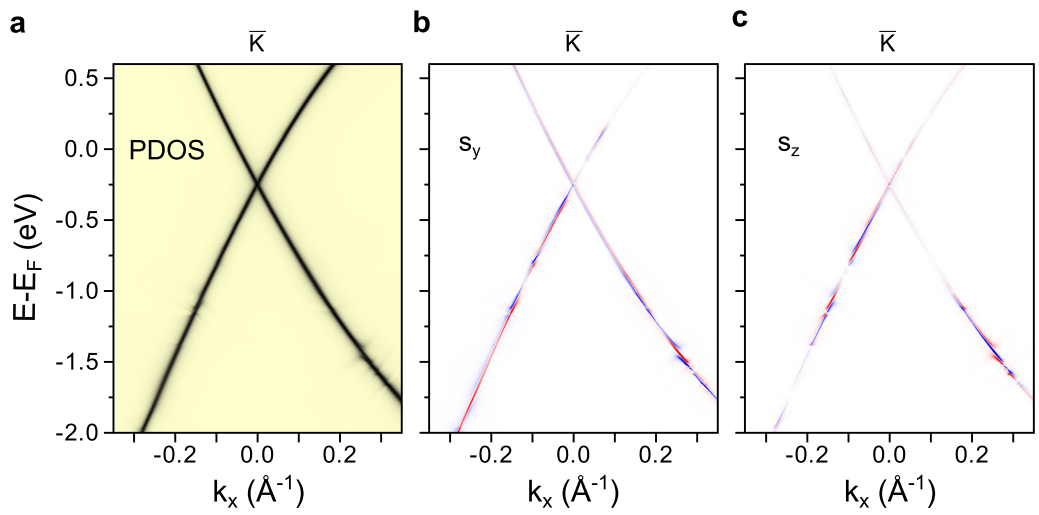

Figure 4. (a) Spin-averaged (k, E)-resolved density of states PDOS(k, E) maps projected onto C atoms of the gr/Pb/Ir(1 1 1) semi-infinite surface system after unfolding from the (10×10) supercell to the graphene (1×1) unit cell. The spectrum is centered at graphene's $\overline{\text{K}}$ point. Panels (b) and (c) show the corresponding in-plane and out-of-plane spin density maps $s(k, E)$.

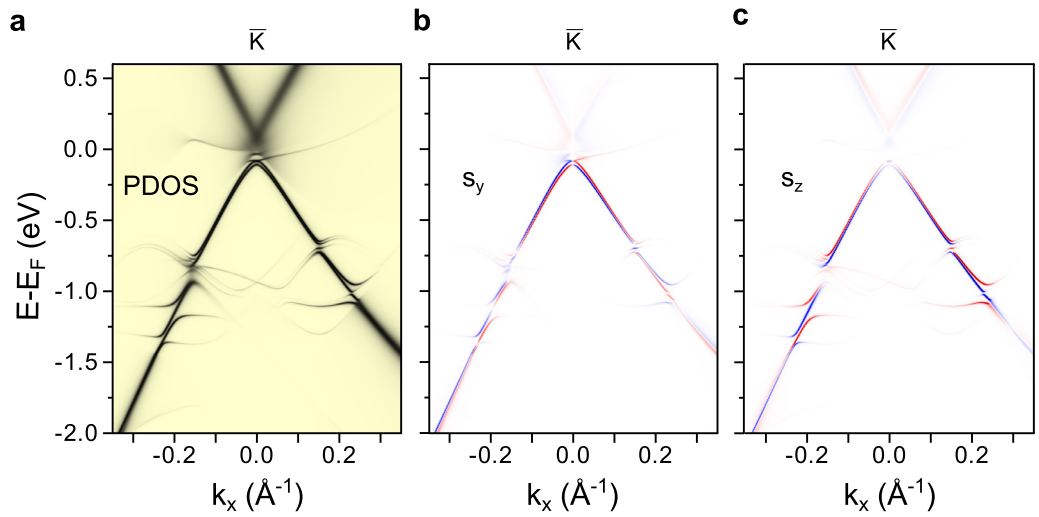

Figure 5. The same as in figure 4, but for the gr/Ir(1 1 1) system.

graphene bands for the Pb-C top and hollow registries is explained in the supplementary note VIII using a model Hamiltonian approach. Additionally, a calculation using a large gr/Pb (10×10) supercell confirms that the average over many different Pb-C registries preserves sublattice symmetry, whereby no out-of-plane spin component is induced by the Pb layer on its own (see supplementary note IX).

For gr*/Pb/Ir(1 1 1), the situation dramatically changes, as compared to gr*/Pb only, due to the strong Pb–Ir hybridization of bands. A clear reminiscence of the linearly dispersive bands near the DP is observed (see figure 7, where the hollow registry case is shown). Incidentally, this hybridization between graphene and Pb/Ir(1 1 1) states is visible in the Pb and Ir projections for all the three different Pb-C registries considered (the top and bridge registries are not shown). This means that the graphene Dirac state is hybridized with both Pb and Ir states. The magnitude of the calculated spin–orbit splittings for gr*/Pb/Ir(1 1 1) using the $c(4 \times 2)$ supercell is of the order of 30–40 meV close to the DP (see figure 8), i. e. comparable to the calculated values in the (10×10) supercell after unfolding. Remarkably, with inclusion of the Ir(1 1 1) substrate, the out-of-plane spin polarization in the C projections appears for all the three Pb-C registries considered, no matter whether sublattice symmetry is broken or not, contrary to the case of gr*/Pb unsupported bilayer discussed before (see figures 8 and 6(a), (b)). All these observations for gr*/Pb only and gr*/Pb/Ir(1 1 1) using the $c(4 \times 2)$ cell's BZ permit us to confirm that the non-planar spin texture in Pb-intercalated graphene is induced by the coupling with Pb/Ir(1 1 1) states carrying out-of-plane spin polarization. However, since the Pb layer in the (10×10) structure does not induce the out-of-plane spin components on its own, one can attribute the origin of the vertical spin polarization induced in graphene to the surface and resonance

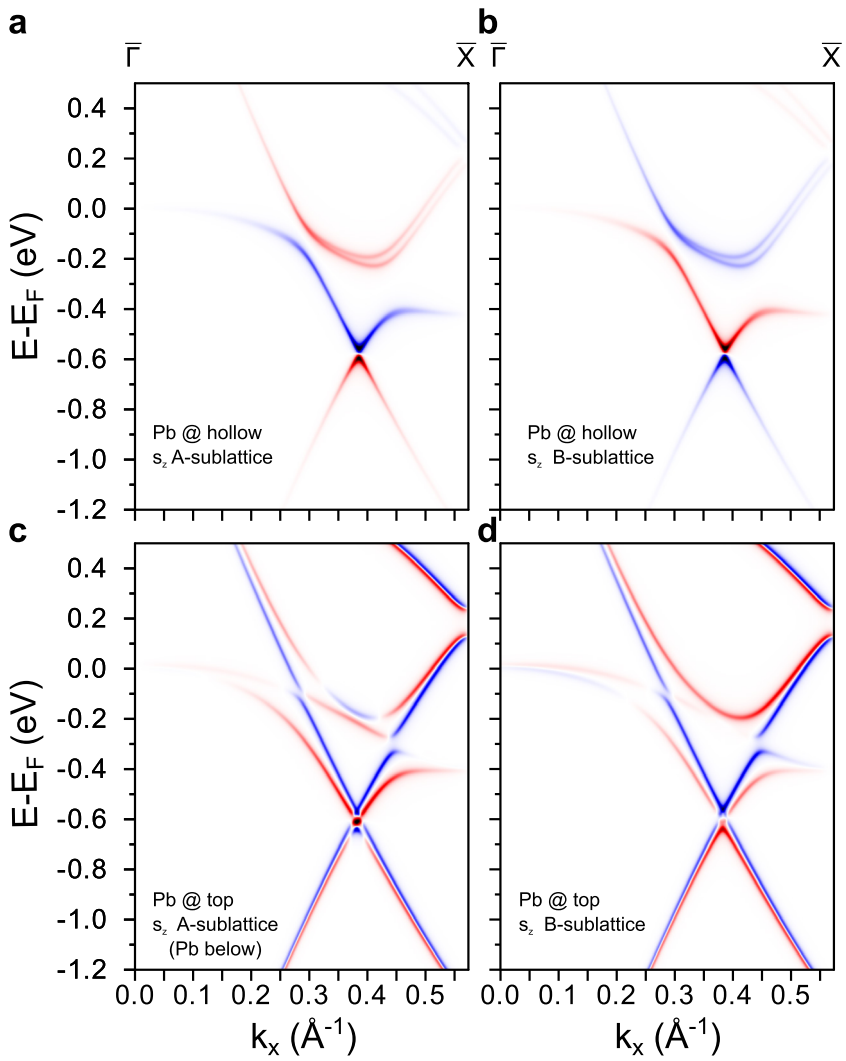

Figure 6. Graphene-projected (k, E)-resolved out-of-plane spin density maps $s_z(k, E)$ for a gr*/Pb bilayer calculated along the $\overline{\Gamma X}$ direction of the $c(4 \times 2)$ BZ for the hollow ((a) and (b)) and top ((c) and (d)) Pb-C registries. The contributions from the two different graphene sublattices are shown separately to illustrate that only for the top registry these out-of-plane components prevail, while for the hollow registry the two contributions cancelled one another, as it should due to the preservation of sublattice symmetry.

states of Ir(1 1 1), carrying significant out-of-plane spin components (supplementary note VII).

Nevertheless, the intercalated Pb layer plays an essential role in determining the spin–orbit splittings of the graphene bands and the out-of-plane spin texture: it changes the doping from *p* to *n* lowering the Dirac cone below the Fermi level and also introduces a folding of Ir(1 1 1) states that closes the metal's projected band gap, thus allowing for hybridizations between the graphene bands and the Pb/Ir(1 1 1) states (supplementary note VII). Actually, both the S1 and S2 surface states near the $\overline{\text{K}}$ point of the pristine Ir(1 1 1), as well as surface resonances at other locations in the BZ (supplementary note VII), hybridize with Pb states of p_z orbital character. This very fact, not only efficiently transfers SOC to graphene electrons, but also induces out-of-plane spin polarization in both the π and π^* states in *n*-doped graphene for gr/Pb/Ir(1 1 1), as compared to the *p*-doped graphene in gr/Ir(1 1 1) that only shows significant spin polarization in the π state. As discussed above, this is due to the energy broadening induced in the π^* state by hybridization with projected bulk Ir(1 1 1) states above the Fermi level.

Therefore, we conclude that the intercalation of a Pb monolayer between graphene and Ir(1 1 1) not only reduces the overall coupling between graphene and Ir(1 1 1) that translates into an almost negligible structural corrugation and nearly perfect linear dispersion, but it also permits the transfer of SOC from the Pb–Ir substrate to the graphene overlayer.

3. Conclusions

In summary, using angle- and spin-resolved photoemission spectroscopy, scanning tunneling microscopy and density functional theory calculations we have evidenced that strong spin–orbit coupling effects can be induced in graphene by intercalation of Pb atoms in between the carbon sheet and the Ir(1 1 1)

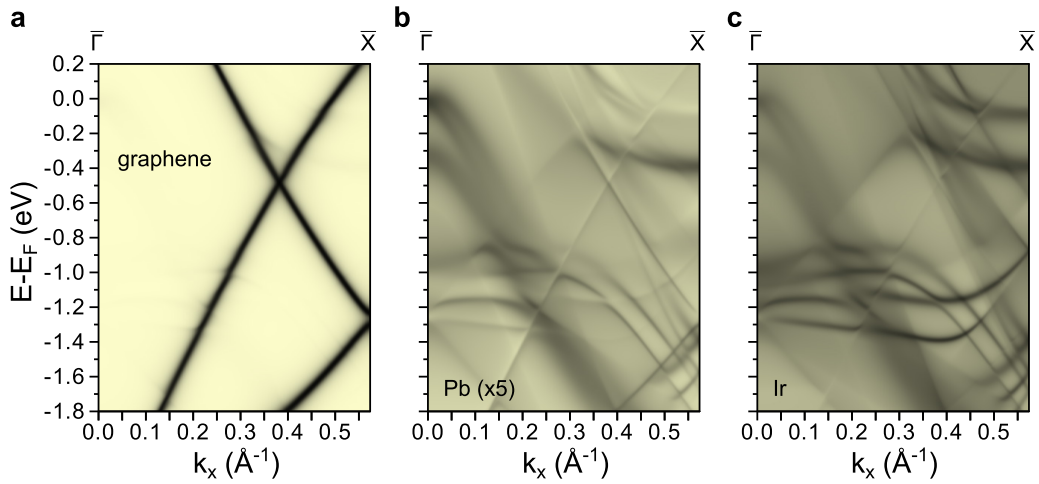

Figure 7. Spin-averaged PDOS(k, E) maps for the gr*/Pb/Ir(1 1 1) semi-infinite surface system as calculated along the $\overline{\Gamma X}$ direction of the $c(4 \times 2)$ cell's BZ for the Pb-C hollow registry. Projections onto the C, Pb and Ir layers are shown in panels (a)–(c), respectively. The Pb-projected PDOS(k, E) is multiplied by 5 for better visualization.

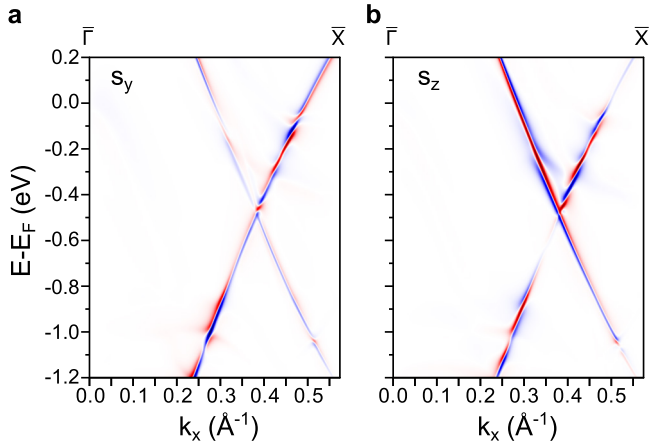

Figure 8. Graphene-projected (k, E)-resolved spin density maps $s(k, E)$ for a gr*/Pb/Ir(1 1 1) semi-infinite surface system calculated along the $\overline{\Gamma X}$ direction of the $c(4 \times 2)$ cell's BZ for the Pb-C hollow registry. Red/blue colors represent positive/negative spin components (a) in-plane along the y and (b) out-of-plane z directions. Notice the appearance of out-of-plane spin component.

substrate, while maintaining the linear dispersion of the π bands. These effects manifest themselves in the emergence of large spin–orbit splittings and intense both in-plane and out-of-plane spin components. Our first principles calculations show that the out-of-plane spin components originate from to the out-of-plane spin-polarized surface and resonance states of Ir(1 1 1), while the Pb interlayer contribution to the vertical spin polarization in the carbon sheet averages to zero. However, the role of the intercalated Pb layer, whose rectangular symmetry imposes the Brillouin zone folding and leads to a closure of the Ir(1 1 1) projected bandgap, appears to be instrumental for the efficient SOC transfer to graphene as well as for the linearization of its bands. The coexistence of both in-plane and out-of-plane spin components in Pb-intercalated graphene on Ir(1 1 1) is consistent with the appearance of an intrinsic SOC of Kane and Mele type that, however, does not exceed the extrinsic Rashba SOC, since no sizable gap has been observed at the Dirac point.

4. Methods

4.1. Experimental

A single monolayer of highly perfect graphene was grown epitaxially on Ir(1 1 1) by exposing the sample to 5×10^{-8} mbar of ethylene at 1300 K. The intercalation of Pb was achieved by evaporating Pb on the gr/Ir(1 1 1) surface kept at 900 K and the sample was finally annealed to 1100 K. STM imaging was employed to verify that the coverage of the Pb intercalated sample was close to 1 monolayer. The STM and ARPES data were recorded in the independent ultra-high vacuum chambers, using LEED as a common characterization technique in order to verify the identical preparation of the samples in the respective experimental chambers.

The angle-resolved photoemission experiments were carried out at the Research Resource Center 'Physical methods of surface investigation' of Saint Petersburg State University. The spin-resolved ARPES measurements were taken at Swiss Light Source at the COPHEE endstation. Energy and momentum reso-

lutions for spin-integrated (spin-resolved) measurements were 15 meV and 0.01 Å^{-1} (50 meV and 0.03 Å^{-1}), respectively. The presented spin polarization projections are given in the sample coordinate frame, with the assumption of $P_x = 0$ since our DFT calculations revealed no s_x component of the spin along the k_x direction. The spin-up and spin-down spectra, used for the splitting estimation were obtained for the spin polarization projection on the axis, co-directed with the spin polarization vector. No averaging was applied to the data. Detailed description of the data treatment is presented in supplementary note X.

4.2. Theoretical

Density functional theory calculations were performed using the generalized gradient approximation to the exchange and correlation potential in the Perdew–Burke–Ernzernhof version [53]. Structural optimizations were performed using the VASP code [54–56] within the projector augmented wave method [57]. The Hamiltonian contained the scalar relativistic corrections and the SOC was taken into account by the second variation method [58]. The energy cut-off in the plane wave expansion was set to 400 eV. The relaxed Ir lattice parameter is equal to 2.737 Å. The atomic structure of the Pb/(1 1 1) was optimized using the $c(4 \times 2)$ in-plane supercell containing 7 Ir layers with 4 Ir atoms per layer. A Pb atom was placed above the topmost surface of the Ir film at top, bridge, fcc and hcp hollow sites and its height was optimized together with all Ir atoms coordinates in the topmost three layers, while the rest of them we fixed at their bulk positions. For the relaxations, a conjugate-gradient algorithm and a force tolerance criterion for convergence of 0.03 eV Å^{-1} were used. To estimate the graphene-Pb/Ir(1 1 1) adsorption distance, we performed static total-energy calculations for 20 different distances between the substrate and graphene layer in three cases—gr/Pb, gr*/Pb, and gr*/Pb/Ir (gr* stays for a stretched graphene, see main text for further details). We explored different registries of the Pb atoms with respect to the graphene honeycomb lattice, namely hollow, bridge, and top (supplementary note IV). In order to describe the van der Waals interactions we made use of the DFT-D2 approach [59]. From the results of these calculations, we conclude that graphene is physisorbed on the Ir-supported Pb layer at a distance of about 3.3–3.4 Å from the Pb atoms.

The electronic band structure calculations were performed employing the GREEN code [60] and its interface to the DFT SIESTA [61] package. In a first step, self-consistent Hamiltonians for all supercells were computed using SIESTA including SOC via the fully-relativistic pseudopotential approach [62]. The core electrons were described by norm-conserving pseudopotentials of the Troulliers–Martin type, with core corrections included for the Pb and Ir atoms. The atomic orbital basis set consisted of double-zeta polarized numerical orbitals that were strictly localized—we set the confinement energy in the basis generation process to 100 meV. Real space three-center integrals were computed over 3D-grids with a resolution of 0.06 Å^3 (equivalent to 700 Rydbergs mesh cut-off) while for the BZ integration the k-meshes of up to 30×30 relative to the Ir (1×1) cell's BZ were employed. The electronic temperature k_BT in the Fermi–Dirac distribution was set to 25 meV. In all the electronic structure calculations the graphene layer was fixed at a distance of 3.4 Å above the Pb layer (or 3.5 Å above the surface Ir layer for the gr/Ir case). The graphene layer was maintained flat (uncorrugated) in order to calculate unfolded graphene-projected band structures [42, 49].

For those systems involving the Ir substrate, a Green's function based approach was followed in order to model the surface as a semi-infinite medium [60]. The electronic and spin structures were then extracted in the form of the graphene-projected density of states, PDOS(k, E), and spin, $s_{x/y/z}(k, E)$, maps. Furthermore, for the (10×10) periodicity calculations, and in order to disentangle the complex graphene-projected band structure resulting from the back-folding, we assumed the graphene layer to preserve a perfect (1×1) periodicity, thus allowing to unfold its π-bands onto the graphene's primitive BZ. The details of the unfolding procedure can be found in [42, 49].

Acknowledgments

We acknowledge the support by the Basque Departamento de Educacion, UPV/EHU (Grant No. IT-756-13), Spanish Ministerio de Economia y Competitividad (MINECO Grants No. FIS2016-75862-P, MAT2015-66888-C3-1R and FIS2015-67367-C2-1-P), Comunidad de Madrid (MAD2D-CM and Nanofrontmag) and Tomsk State University competitiveness improvement programme (project No. 8.1.01.2017). The support by the Saint Petersburg State University (Grant No. 15.61.202.2015) and Russian Foundation for Basic Research (Grant No. 18-32-00145) are also acknowledged. The part of photoemission measurements had been supported by Russian Science Foundation Grant No. 18-12-00062. IMDEA Nanociencia acknowledges support from the 'Severo Ochoa' Programme for Centres of Excellence in R&D (MINECO, Grant SEV-2016-0686). The calculations were performed in Donostia International Physics Center and in the Research park of St. Petersburg State University Computing Center (http://cc.spbu.ru).

ORCID iDs

M M Otrokov https://orcid.org/0000-0001-5775-3386
I I Klimovskikh https://orcid.org/0000-0003-0243-0322
A M Shikin https://orcid.org/0000-0002-2476-1248
O Vilkov https://orcid.org/0000-0002-8984-8790
A G Rybkin https://orcid.org/0000-0002-8237-4959

References

[1] Manchon A, Koo H C, Nitta J, Frolov S and Duine R 2015 *Nat. Mater.* **14** 871–82
[2] Soumyanarayanan A, Reyren N, Fert A and Panagopoulos C 2016 *Nature* **539** 509–17
[3] Kane C L and Mele E J 2005 *Phys. Rev. Lett.* **95** 226801
[4] Bernevig B A, Hughes T L and Zhang S C 2006 *Science* **314** 1757–61
[5] König M, Wiedmann S, Brüne C, Roth A, Buhmann H, Molenkamp L W, Qi X L and Zhang S C 2007 *Science* **318** 766–70
[6] Qi X L, Hughes T L and Zhang S C 2008 *Phys. Rev.* B **78** 195424
[7] Chang C Z *et al* 2013 *Science* **340** 167–70
[8] Krieger J A *et al* 2017 *Phys. Rev.* B **96** 184402
[9] Kitaev A Y 2001 *Phys.-Usp.* **44** 131
[10] Fu L and Kane C L 2008 *Phys. Rev. Lett.* **100** 096407
[11] Mourik V, Zuo K, Frolov S M, Plissard S, Bakkers E and Kouwenhoven L P 2012 *Science* **336** 1003–7
[12] Fert A, Cros V and Sampaio J 2013 *Nat. Nanotechnol.* **8** 152–6
[13] Heinze S, Von Bergmann K, Menzel M, Brede J, Kubetzka A, Wiesendanger R, Bihlmayer G and Blügel S 2011 *Nat. Phys.* **7** 713–8
[14] Roldán R, López-Sancho M, Guinea F, Cappelluti E, Silva-Guillén J and Ordejón P 2014 *2D Mater.* **1** 034003
[15] Kormányos A, Burkard G, Gmitra M, Fabian J, Zólyomi V, Drummond N D and Fal'ko V 2015 *2D Mater.* **2** 022001
[16] Otrokov M M *et al* 2017 *2D Mater.* **4** 025082
[17] Lado J L and Fernandez-Rossier J 2017 *2D Mater.* **4** 035002
[18] Gmitra M, Kochan D, Högl P and Fabian J 2016 *Phys. Rev.* B **93** 155104
[19] Marchenko D, Sánchez-Barriga J, Scholz M R, Rader O and Varykhalov A 2013 *Phys. Rev.* B **87** 115426
[20] Avsar A *et al* 2014 *Nat. Commun.* **5** 4875
[21] Klimovskikh I I, Tsirkin S S, Rybkin A G, Rybkina A A, Filianina M V, Zhizhin E V, Chulkov E V and Shikin A 2014 *Phys. Rev.* B **90** 235431
[22] Shikin A M, Rybkina A A, Rybkin A G, Klimovskikh I I, Skirdkov P N, Zvezdin K A and Zvezdin A K 2014 *Appl. Phys. Lett.* **105** 042407
[23] Marchenko D, Varykhalov A, Scholz M R, Bihlmayer G, Rashba E I, Rybkin A, Shikin A M and Rader O 2012 *Nat. Commun.* **3** 1232
[24] Calleja F *et al* 2015 *Nat. Phys.* **11** 43–7
[25] Klimovskikh I I, Vilkov O, Usachov D Y, Rybkin A G, Tsirkin S S, Filianina M V, Bokai K, Chulkov E V and Shikin A M 2015 *Phys. Rev.* B **92** 165402
[26] Klimovskikh I I, Otrokov M M, Voroshnin V Y, Sostina D, Petaccia L, Di Santo G, Thakur S, Chulkov E V and Shikin A M 2017 *ACS Nano* **11** 368–74
[27] Estyunin D A, Klimovskikh I I, Voroshnin V Y, Sostina D M, Petaccia L, Santo G D and Shikin A M 2017 *JETP* **125** 762–7
[28] Klimovskikh I I, Otrokov M M, Voroshnin V Y, Sostina D, Petaccia L, Di Santo G, Thakur S, Chulkov E V and Shikin A M 2017 *ACS Nano* **11** 10630–2
[29] Weeks C, Hu J, Alicea J, Franz M and Wu R 2011 *Phys. Rev.* X **11** 021001
[30] Ma D and Yang Z 2011 *New J. Phys.* **13** 123018
[31] Brey L 2015 *Phys. Rev.* B **92** 235444
[32] Varykhalov A, Sánchez-Barriga J, Marchenko D, Hlawenka P, Mandal P and Rader O 2015 *Nat. Commun.* **6** 7610
[33] Rashba E I 2009 *Phys. Rev.* B **79** 161409
[34] Gmitra M, Konschuh S, Ertler C, Ambrosch-Draxl C and Fabian J 2009 *Phys. Rev.* B **80** 235431
[35] Abdelouahed S, Ernst A, Henk J, Maznichenko I V and Mertig I 2010 *Phys. Rev.* B **82** 125424
[36] Vo P T, Walet N R and Guinea F P 2017 *2D Mater.* **5** 014004
[37] Qiao Z, Yang S A, Feng W, Tse W K, Ding J, Yao Y, Wang J and Niu Q 2010 *Phys. Rev.* B **82** 161414
[38] Garcia-Lekue A, Balashov T, Olle M, Ceballos G, Arnau A, Gambardella P, Sanchez-Portal D and Mugarza A 2014 *Phys. Rev. Lett.* **112** 066802
[39] Usachov D *et al* 2015 *Nano Lett.* **15** 2396–401
[40] Usachov D Y *et al* 2015 *ACS Nano* **9** 7314–22
[41] Usachov D Y *et al* 2016 *Nano Lett.* **16** 4535–43
[42] Brede J, Sławińska J, Abadia M, Rogero C, Ortega J E, Piquero-Zulaica I, Lobo-Checa J, Arnau A and Cerdá J I 2017 *2D Mater.* **4** 015016
[43] Rybkin A G *et al* 2018 *Nano Lett.* **18** 1564–74
[44] He P, Zhang S S L, Zhu D, Liu Y, Wang Y, Yu J, Vignale G and Yang H 2018 *Nat. Phys.* **14** 495–9
[45] N'Diaye A T, Coraux J, Plasa T N, Busse C and Michely T 2008 *New J. Phys.* **10** 043033
[46] Rutter G M, Crain J N, Guisinger N P, Li T, First P N and Stroscio J A 2007 *Science* **317** 219–22
[47] Mallet P, Varchon F, Naud C, Magaud L, Berger C and Veuillen J Y 2007 *Phys. Rev.* B **76** 041403
[48] Warmuth J, Bruix A, Michiardi M, Hänke T, Bianchi M, Wiebe J, Wiesendanger R, Hammer B, Hofmann P and Khajetoorians A A 2016 *Phys. Rev.* B **93** 165437
[49] Slawinska J and Cerda J 2017 arXiv:1709.02305
[50] Pletikosić I, Kralj M, Pervan P, Brako R, Coraux J, N'Diaye A T, Busse C and Michely T 2009 *Phys. Rev. Lett.* **102** 056808
[51] Kralj M, Pletikosić I, Petrović M, Pervan P, Milun M, N'Diaye A T, Busse C, Michely T, Fujii J and Vobornik I 2011 *Phys. Rev.* B **84** 075427
[52] Rakyta P, Kormányos A and Cserti J 2011 *Phys. Rev.* B **83** 155439
[53] Perdew J P, Burke K and Ernzerhof M 1996 *Phys. Rev. Lett.* **77** 3865–8
[54] Kresse G and Furthmüller J 1996 *Phys. Rev.* B **54** 11169–86
[55] Kresse G and Joubert D 1999 *Phys. Rev.* B **59** 1758–75
[56] Kresse G and Hafner J 1993 *Phys. Rev.* B **47** 558–61
[57] Blöchl P E 1994 *Phys. Rev.* B **50** 17953–79
[58] Koelling D D and Harmon B N 1977 *J. Phys. C: Solid State Phys.* **10** 3107
[59] Grimme S 2006 *J. Comput. Chem.* **27** 1787–99
[60] Rossen E T R, Flipse C F J and Cerdá J I 2013 *Phys. Rev.* B **87** 235412
[61] Soler J M, Artacho E, Gale J D, García A, Junquera J, Ordejón P and Sánchez-Portal D 2002 *J. Phys.: Condens. Matter* **14** 2745
[62] Cuadrado R and Cerdá J 2012 *J. Phys.: Condens. Matter* **24** 086005